*Journal of Applied Mechanics and Technical Physics, Vol. 49, No. 1, pp. 9–17, 2008*

# CHARGE TRANSFER BY HIGH-ENERGY ELECTRONS ONTO THE LEEWARD SURFACES OF A SOLID IN A SUPERSONIC RAREFIED PLASMA FLOW

**V. A. Shuvalov, A. I. Priimak, K. A. Bandel, and G. S. Kochubei**

UDC 533.95

*Numerical and experimental dependence of equilibrium potentials of the leeward surfaces on the ratio of concentrations of high-energy electrons and positive ions in a supersonic rarefied plasma flow around a solid are obtained.*

**Key words:** *plasma, solid, supersonic flow, electrons, equilibrium potential.*

**Introduction.** Electrodynamic interaction of solids with the polar ionosphere in the Earth's shadow is a superposition of two effects: irradiation by high-energy electrons and the flow of a "cold" rarefied plasma. If the concentration of positive ions near the body surface is $N_{iw} \leqslant 10^4$ cm$^{-3}$, negative charges up to a voltage of 1 kV are collected on the dielectric [1]. The main role in charging the solid surfaces in the polar ionosphere in the Earth's shadow belongs to hot electrons with energy from 1 to 35 keV (captured in radiation belts and propagating along the lines of magnetic force toward the Earth surface) and positive ions of the "cold" ionospheric plasma. The effects and consequences of high-voltage differential charging are most hazardous for the leeward surfaces of extended and electrodynamically large solids ($R/\lambda_{ds} > 10$) and also for small solids in the near wake behind them [$R$ is the characteristic size of the solid; $\lambda_{ds} = \sqrt{kT_{es}/(4\pi e^2 N_{es})}$ is the Debye screening length of the undisturbed plasma, $k$ is the Boltzmann constant, $e$ is the electron charge, $T_{es} \leqslant 0.3$ eV is the temperature, and $N_{es}$ is the concentration of electrons in the "cold" plasma].

The numerical study of high-voltage charging of the leeward surfaces of a solid in a polar plasma involves the solution of nonlinear integrodifferential Vlasov–Poisson equations for a supersonic flow and current-balance equations on the irradiated surface. The values of the coefficients of interaction between the charged particles and the surface for a particular material are determined experimentally.

In the experimental study of high-voltage charging, it is necessary to reproduce the current density distribution in the near wake behind the solid in a supersonic rarefied plasma flow and simultaneous irradiation of the leeward surfaces by high-energy electrons with energy from 1 to 35 keV [1]. The test set designed for such studies has to combine the characteristics of a plasma gas-dynamic tunnel and an electrodynamic facility. The conditions of charging of dielectric solids in a polar plasma can be modeled (simulated) in a closed volume of such a test set. The difficulties of such studies are caused by the necessity of simultaneous implementation of conditions of plasma-gas-dynamic and electrophysical interactions in the solid–plasma system. The accuracy and reliability of the predicted level of charging of the leeward surfaces are determined by the agreement between the calculated values of the solid potentials and the data of ionospheric and test-set measurements.

In the near wake behind an electrodynamically large solid, the concentration of positive ions of the "cold" plasma $N_{is}$ is several orders lower than its value $N_{i\infty}$ in the undisturbed plasma with an almost unchanged concentration of high-energy electrons $N_{eh}$. This fact and also the nonuniform distribution of charge density over the

Institute of Mechanical Engineering, Ukrainian National Academy of Sciences, Dnepropetrovsk, Ukraine 49005; shuv@vash.dp.ua. Translated from Prikladnaya Mekhanika i Tekhnicheskaya Fizika, Vol. 49, No. 1, pp. 13–23, January–February, 2008. Original article submitted March 6, 2007.

near-wake cross section and on the dielectric surface of the solid create conditions for differential charging of the leeward surfaces. If the difference of potentials is equal or close to the threshold values of breakdown potentials of dielectric materials, radiation-stimulated breakdowns, surface electric discharges, and formation of conductivity channels with ejection of the plasma of the solid and electromagnetic radiation, i.e., fracture of materials, are highly probable.

**Parameters of Similarity and Criterial Relations.** Interaction of solids with a rarefied plasma under conditions of a supersonic collisionless flow is characterized by the Vlasov system of kinetic equations for each component of the plasma and by the Maxwell equations for a self-consistent field with the boundary conditions set in the undisturbed medium and on the solid surface. The solution of the steady-state problem of the rarefied plasma flow around a solid is defined by the following scale coefficients [2]: ratio of the velocity of motion of the solid $U_\infty$ to the velocity of ion sound $V_{is} = \sqrt{2kT_{es}/M_i}$ ($M_i$ is the ion mass) $S_{ei} = U_\infty/\sqrt{2kT_{es}/M_i}$, ratio of the characteristic size of the solid $R$ to the Debye screening length $\lambda_{ds}$ of the undisturbed plasma $R_{ds} = R/\lambda_{ds}$, dimensionless potential of the solid $\Phi_w = e\varphi_w/(kT_{es})$ ($\varphi_w = \varphi_0 - \varphi_p$ is the potential of the solid $\varphi_0$ relative to the potential of the plasma $\varphi_p$), ratio of the characteristic size of the solid to the Larmor radius of the charged particles $R/\rho_\alpha$ [$\rho_\alpha = M_\alpha V_\alpha c/(e_\alpha H)$, where $c$ is the velocity of light, $V_\alpha$ if the particle velocity and $H$ is the magnetic field strength; $\alpha \equiv e, i$, where the subscripts $e$ and $i$ refer to electrons and ions, respectively], and degree of plasma nonisothermality $\xi_{ei} = T_{es}/T_{is}$ (ratio of the electron $T_{es}$ and ion $T_{is}$ temperatures). The ratio $2e\varphi_w/(M_iU_\infty^2)$ or $\Phi_w/S_{ei}^2$ is sometimes used in addition to the parameters of similarity mentioned above.

The study of the electrophysical aspect of interaction between the solid and the polar plasma is based on similarity of electric and magnetic fields of the solid under the action of high-energy electrons. The electromagnetic processes in the solid are characterized by a system of the Maxwell equations, which yields five parameters of similarity [3]:

$$\Pi_1 = \frac{gE}{N_{eh}V_{eh}}, \quad \Pi_2 = \frac{\varepsilon E}{N_{eh}V_{eh}\tau}, \quad \Pi_3 = \frac{N_{eh}\Lambda}{\varepsilon E}, \quad \Pi_4 = \frac{H}{N_{eh}V_{eh}\Lambda}, \quad \Pi_5 = \frac{\tau E}{\mu\Lambda H}. \tag{1}$$

Here $g$ is the specific conductivity of the material, $E$ and $H$ are the strengths of the electric and magnetic fields in the material, $N_{eh}$ and $V_{eh}$ are the concentration and velocity of high-energy electrons, $\varepsilon$ and $\mu$ are the dielectric and magnetic permeabilities of the material, $\Lambda$ is the characteristic size of the material, and $\tau$ is the characteristic time of the process.

In the polar plasma in the Earth's shadow, the equilibrium potential on the leeward side of the dielectric solid is determined from the balance equation for currents of high-energy electrons and charged particles of the "cold" rarefied plasma:

$$\sum j_\beta(\varphi_w) = j_{e\beta} - (j_{iw} + j_{er\beta} + j_{eb\beta} + j_{ie}) = 0. \tag{2}$$

Here $j_{e\beta}$ is the current density of the electrons affecting the surface ($\beta \equiv s, h$, where the subscripts $s$ and $h$ refer to the "cold" and "hot" electrons, respectively), $j_{iw}$ is the current density of ions of the "cold" plasma, $j_{er\beta}$ is the current density of secondary electrons, $j_{eb\beta}$ is the current density of backward scattered electrons, and $j_{ie}$ is the current density of secondary ion-electron emission.

The current density of high-energy electrons in the polar plasma is $j_{eh}$ = 1–10 nA/cm$^2$ [1]. The current density of high-energy electrons in the near wake behind the solid remains almost constant [4]. Their energy is substantially greater than the energy of ions and electrons of the "cold" plasma in the ionosphere. Collection of "cold" electrons $j_{es} = eN_{es}\sqrt{kT_{es}/(2\pi m_e)}\exp(\Phi_w)$ by a negatively charged solid at $\Phi_w \gg 10$ is negligible. The balance equation of the currents of charged particles on the leeward surface of the solid (2) is written in the form

$$\sum j_\alpha(\varphi_w) = (1-\sigma_{eh})eN_{eh}\sqrt{\frac{kT_{eh}}{2\pi m_e}}\ \exp\left(\frac{e\varphi_w}{kT_{eh}}\right) - (1+\gamma_i)j_{iw} = 0, \tag{3}$$

where $\sigma_{eh}$ is the coefficient of the secondary electron emission of high-energy electrons and $\gamma_i$ is the coefficient of the secondary ion-electron emission.

Six parameters of similarity of plasma-gas-dynamic interaction ($S_{ei}$, $R_{ds}$, $\Phi_w$, $R/\rho_i$, $R/\rho_e$, and $\xi_{ei}$), the parameter of geometric modeling $\beta = R_{\rm mod}/R_{\rm el}$ ($R_{\rm mod}$ and $R_{\rm el}$ are the characteristic sizes of the model and element of the structure, respectively), the Knudsen number Kn = $\lambda_{ii}/R$ ($\lambda_{ii}$ is the mean free path for ion–ion collisions), and five parameters of similarity of electrophysical interaction (1) define the requirements to the accuracy

and purity of arrangement of the physical experiment and allow formulating the criteria that establish the relation between the parameters of interaction in the solid–plasma system on the test set and in the polar plasma.

The scale coefficients characterizing the plasma-gas-dynamic interaction for solids with the characteristic size $R_{\rm el} = 0.5$ m at $U_\infty \approx 7.5$ km/sec at altitudes of 300 to 1000 km acquire the values $3.3 \leqslant S_{ei} \leqslant 6.0$, $30 \leqslant R_{ds} \leqslant 210$, $T_{is}/T_{es} = 0.25$–$1.00$, and $R_{\rm el}/\rho_{es} = 10$–$15$.

The laboratory plasma is substantially nonisothermal; therefore, the electron temperature $T_{es}^{(\rm mod)}$ of the "cold" laboratory plasma flow can be reasonably used in analyzing the results of set tests of a supersonic flow around a solid. Using a fixed ratio of temperatures $T_{es}^{(\rm mod)}/T_{es}^{(\rm nat)} = \xi_{es}$ and the scale coefficients $R_{ds}$, $S_{ei}$, and $R/\rho_{es}$, we obtain the criterial relations for the concentration of charged particles, particle velocity, and strength of the external magnetic field:

$$\frac{N_{es}^{(\rm mod)}}{N_{es}^{(\rm nat)}} = \xi_{es}\beta^{-2}, \qquad \frac{U_\infty^{(\rm mod)}}{U_\infty^{(\rm nat)}} = \Big(\frac{\xi_{es}}{b}\Big)^{1/2}, \qquad \frac{H^{(\rm mod)}}{H^{(\rm nat)}} \approx \frac{\xi_{es}^{1/2}}{\beta}. \tag{4}$$

Here the superscripts "mod" and "nat" refer to parameters of the laboratory-scale model plasma flow and natural ionospheric plasma; $b = M_i^{(\rm mod)}/M_i^{(\rm nat)}$.

The basic species in the ionospheric plasma at altitudes of 300 to 1000 km is ionized atomic oxygen; with allowance for the parameters of the "cold" ionospheric plasma [1], the criterial relations (4) with $\xi_{es} \geqslant 3$ yield $10^5$ cm$^{-3} \leqslant N_{is}^{(\rm mod)} \leqslant 10^7$ cm$^{-3}$, $U_\infty^{(\rm mod)} \geqslant 11.1$ km/sec, and $H^{(\rm mod)} \geqslant 2.4 \cdot 10^3$ A/m.

For adequate conditions of the charging process, collection of the high-voltage charge, and identical velocities (energies) of high-energy electrons, and for identical dielectric materials used on the test set and in the ionosphere tests with allowance for the relations $j_{eh}^{(\rm mod)} \neq j_{eh}^{(\rm nat)}$ and $N_{eh}^{(\rm mod)} \neq N_{eh}^{(\rm nat)}$, the parameters of similarity (1) yield the criterial relations for the strengths of the electric and magnetic fields in the dielectric and the characteristic time of charging:

$$E^{(\rm nat)} = \frac{N_{eh}^{(\rm nat)}}{N_{eh}^{(\rm mod)}}\, E^{(\rm mod)}, \qquad H^{(\rm nat)} = \frac{N_{eh}^{(\rm nat)}}{N_{eh}^{(\rm mod)}}\, H^{(\rm mod)}, \qquad \tau^{(\rm mod)} = \tau^{(\rm nat)}. \tag{5}$$

If the conditions of electrophysical forcing for identical dielectric materials are reached on the test set and identical strength of the breakdown electric field is reached, Eq. (1) yields

$$j_{eh}^{(\rm mod)} = j_{eh}^{(\rm nat)}, \quad V_{eh}^{(\rm mod)} = V_{eh}^{(\rm nat)}, \quad N_{eh}^{(\rm mod)} = N_{eh}^{(\rm nat)}, \quad \tau^{(\rm mod)} = \tau^{(\rm nat)}, \quad H^{(\rm mod)} = H^{(\rm nat)}. \tag{6}$$

The balance equation of current density on the leeward side of the dielectric (2) yields the relations for the current densities of positive ions of the "cold" ionospheric and laboratory plasma:

— for conditions (5),

$$\frac{j_{eh}^{(\rm mod)}}{j_{eh}^{(\rm nat)}} = \frac{N_{eh}^{(\rm mod)}}{N_{eh}^{(\rm nat)}} = \frac{j_{iw}^{(\rm mod)}}{j_{iw}^{(\rm nat)}} = \zeta_{eh};$$

— for conditions (6),

$$j_{iw}^{(\rm mod)} = j_{iw}^{(\rm nat)} \qquad (\zeta_{eh} = 1).$$

**Interaction of a Solid with a Supersonic Rarefied Plasma Flow.** The motion in the polar ionosphere occurs with a velocity $V_{is} \ll U_\infty \ll V_{es}$ ($V_{\alpha s}$ is the thermal velocity of charged particles) in a strongly rarefied medium, where the mean free path of particles is much greater than the characteristic size of the solid ($R \gg \lambda_\alpha$), and the Debye screening length is small, as compared with the linear size of the solid ($\lambda_{ds} < R$). Under such conditions, the problem of the near-wake structure includes several small parameters of similarity ($S_e = U_\infty/V_{es}$, $S_i^{-1} = V_{is}/U_\infty$, and $R_{ds}^{-1} = \lambda_{ds}/R$) and reduces to solving the equation

$$\Delta\Phi = R_{ds}^2\{n_{is}[\Phi(\boldsymbol{r})] - \exp[\Phi(\boldsymbol{r})]\} \tag{7}$$

with the boundary conditions [5]

$$\Phi(\infty) = 0, \qquad \Phi(R) = \Phi_w. \tag{8}$$

With allowance for the influence of the electric field on the motion of ions in a solid-fitted system, we can use the integral dependences $n_{is}[\Phi(\boldsymbol{r})]$ from [6] for the current density of ions in the near wake behind an axisymmetric

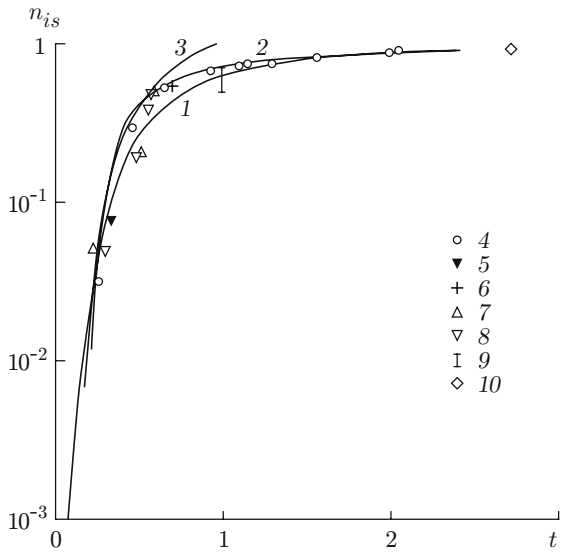


Fig. 1. Normalized ion current density on the axis of the near wake behind a sphere: curve 1 is the solution of Eq. (7) with the dependence $n_{is}(\Phi)$ from [6] with $S_{ei} = 4.5$, $\xi_{ei} = 1$, $R_{ds} \approx 101$, and $-\Phi_w = 3$; curves 2 and 3 are the results of calculations by formulas (69) and (73) from [2], respectively, with $\xi_{ei} = 4$ and with a spherical shape correction; points 4 refer to the results measured in the present work for $S_{ei} = 4.3$, $\xi_{ei} \approx 4$, $R_{ds} \approx 117$, and $-\Phi_w = 1.8$; points 5–8 refer to the results measured in [8] for $S_{ei} = 8.83$, $R_{ds} \approx 14$, $-\Phi_w = 5$, and $\xi_{ei} \geqslant 5$ (5), $S_{ei} = 8.37$, $R_{ds} \approx 50$, $\Phi_w \approx 0$, and $\xi_{ei} = 2$ (6), $S_{ei} \approx 8.06$, $R_{ds} \approx 30$, $\Phi_w \approx 0$, and $\xi_{ei} \geqslant 5$ (7), and $S_{ei} \approx 7.4$, $R_{ds} \approx 10$, $-\Phi_w \approx 1.0$, and $\xi_{ei} \geqslant 5$ (8); points 9 are the results measured in [2] in the ionosphere of the Arieĺ-1 artificial satellite for $S_{ei} = 5$, $R_{ds} \approx 10$, $-\Phi_w \approx 6$, and $\xi_{ei} \approx 1$; points 10 are the results measured in [9] in the wake behind a sphere for $S_{ei} = 5.7$, $R_{ds} \approx 26$, $-\Phi_w \approx 3$, and $\xi_{ei} = 1$.

solid (sphere). The integral dependences (69) and (73) from [2] can be used for $n_{is}$ in the wake behind a disk for $-\Phi_w \leqslant 3$. The real shape of the solid affects the distribution of ions in the near wake at $t \leqslant S_{ei}^{-2/3}$ [$t = z/(RS_{ei})$, where $z$ is the axial coordinate in the near wake behind the solid]. In calculating $n_{is}$ in the wake behind a sphere by the formulas from [2], one can take into account the real shape of the body by introducing a spherical shape correction: $R_{\text{eff}} = R[1 + 0.5(R/z)^2]$.

In the flow around an infinite cylinder aligned perpendicular to the free-stream velocity vector, the ion current density in the near wake can be described by the integral dependences $n_{is}[\Phi(\boldsymbol{r})]$ derived in [6]. The transition from the plate to the cylinder can be ensured by introducing an effective radius $R_{\text{eff}} = R[1 + 0.5(R/z)^2]^{1/2}$.

Equation (7) with the boundary conditions (8) was solved with the use of the iterative scheme [5].

In set tests of interaction of solids with the "cold" ionospheric plasma, the most important problem is to provide the regime of the flow around a solid of radius $R \geqslant 0.5$ m at altitudes of 150 to 1000 km. There is a certain advantage in gas-discharge accelerators with a hot cathode, which generate quasi-neutral plasma flows with the energy of charged particles from 1 to 100 eV and their concentration in the working part of the jet equal to $10^{16}$–$10^{17}$ m$^{-3}$. The diagnosing, measurement, and monitoring of parameters of high-velocity flows of the nonequilibrium rarefied plasma were performed in this work by means of electric probes, a pressure probe, an MKh 7303 mass spectrometer, and a microwave interferometer operating at a frequency of 5.45 GHz. The measurement technique and the procedure of processing of the output probe signals are described in [7].

The experimental study was performed on a plasma-dynamic set in $O^+ + O_2^+$ plasma jets with a degree of dissociation up to 0.6, $3.1 \leqslant S_{ei} \leqslant 4.5$, $T_{is}/T_{es} \approx 0.25$, $21.3 \leqslant R_{ds} \leqslant 127$, and a negative potential of the solid $\Phi_w \leqslant 10$. In studying the near-wake structure, the axisymmetric solids used were conducting and dielectric spheres and disks made of copper, aluminum, and Plexiglas (polymethylmethacrylate) with their radii ranging from 10 to 30 mm. The normalized ion current density along the near-wake axis $n_{is}(t) = I_i/I_{i\infty}$ ($I_i$ is the strength of the ion current in the near wake and $I_{i\infty}$ is the undisturbed strength of current in the measurement cross section) in a supersonic flow around a sphere with a normalized radius $R/\lambda_{ds} > 10$ is plotted in Fig. 1.

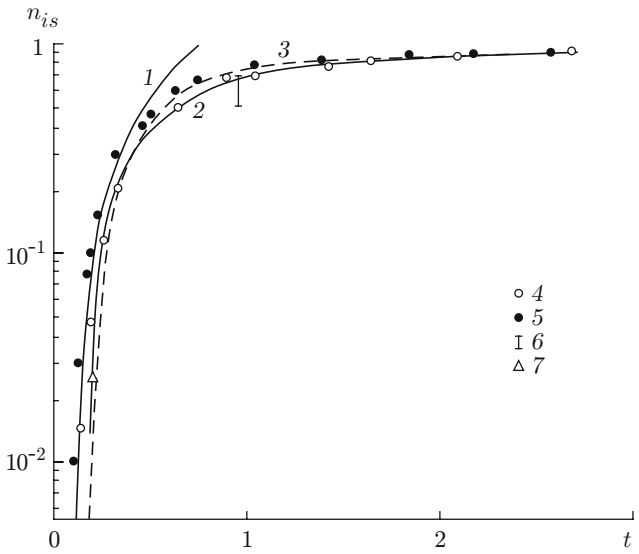


Fig. 2. Dependence $n_{is}(t)$ on the axis of the near wake behind a disk: curves 1 and 3 are the results calculated by formulas (69) and (73) from [2] for $S_{ei} = 3.1$ and $\xi_{ei} = 4$; curve 2 is the solution of Eq. (7) with the dependence $n_{is}(\Phi)$ from [6]; points 4 and 5 are the results measured in the present work for $S_{ei} \approx 3.1$, $R_{ds} \approx 101$, $\xi_{ei} \approx 4$, and $-\Phi_w \approx 3.6$ (4) and 11.2 (5); points 6 are the results measured on the Ariél-1 artificial satellite with recalculation to the disk wake for $S_{ei} \approx 5$, $R_{ds} \approx 10$, $-\Phi_w \approx 6$, and $t \approx 0.96$; points 7 are the results measured in [10] in the wake behind a glass disk for $S_{ei} \approx 3.5$, $R_{ds} \approx 75$, and $-\Phi_w \approx 5$.

The nonisothermality amplifies focusing of positive ions on the axis of the near wake behind the solid. If the solid is not too extended in the free-stream direction, i.e., its longitudinal size is $L \ll RS_{ei}$, then the values $t = z/(RS_{ei})$ corresponding to points on the solid surface are small. The disturbances are determined by the maximum cross section of the solid in the plane orthogonal to the velocity vector $\boldsymbol{U}_\infty$. For $L \ll RS_{ei}$, all bodies of revolution can be replaced by a disk [2].

The distributions of positive ions in the near wake behind a disk were studied in experiments with models made of 12Kh18N10T stainless steel, aluminum, and Plexiglas with radii of 10 to 25 mm and thicknesses of 1–2 mm. The calculated and experimental dependences $n_{is}(t)$ in the near wake behind a disk subjected to a supersonic flow are plotted in Fig. 2. In the range $t \leqslant 0.5$, the results measured for $-\Phi_w \geqslant 10$ are in better agreement with the values of $n_{is}$ calculated by formula (73) from [2]. For $-\Phi_w < 10$ and $t \geqslant 0.25$, the experimental results of the present work and [9] and the ionospheric measurements on the Ariél-1 artificial satellite are closer to the values of $n_{is}$ calculated in [6] and to the values of $n_{is}$ calculated by formula (69) from [2].

The distribution of the ion flow density $n_{is}(t)$ on the axis of the near wake in a supersonic flow around a large flat solid is shown in Fig. 3a. The angular distribution of density of positive ions $n_{is}(\theta)/n_{i\infty} = I_i(\theta)/I_i(0)$ in the near wake behind a flat solid (cylinder) in the "cold" ionospheric plasma is shown in Fig. 3b ($\theta$ is the angle between the radius vector of the point and the axis of symmetry of the wake).

A comparison of the results of set tests and ionospheric measurements shows that the distributions of density of charged particles of the "cold" plasma are consistent with the values obtained on the basis of numerical calculations and near-wake models, which actually validates the accuracy of plasma-dynamic modeling of the near-wake structure in a supersonic flow around a solid by a "cold" rarefied plasma.

**High-Voltage Charging of the Leeward Surfaces of a Solid by High-Energy Electrons in a Rarefied Plasma Flow.** The inhomogeneous structure of the body surface in the ionosphere in set tests was provided by using plates and disks (aluminum, stainless steel, and quartz) with dielectric or metallic coatings. A dielectric coating was applied to one side of the plate made of aluminum (length $l = 45$ cm, width $2R = 16$ cm, and thickness $\delta \approx 0.1$ cm). An aluminum coating was applied (sprayed) onto the surface of the disk (made of quartz) 15 cm in diameter and 0.2 cm thick. The dielectrics were plates made of VPS-7V carbon-based plastic of thickness $\delta \approx 0.18$ cm and a TR-SO-11 thermoradiation coating [consisting of a layer of enamel (zinc oxide) and a

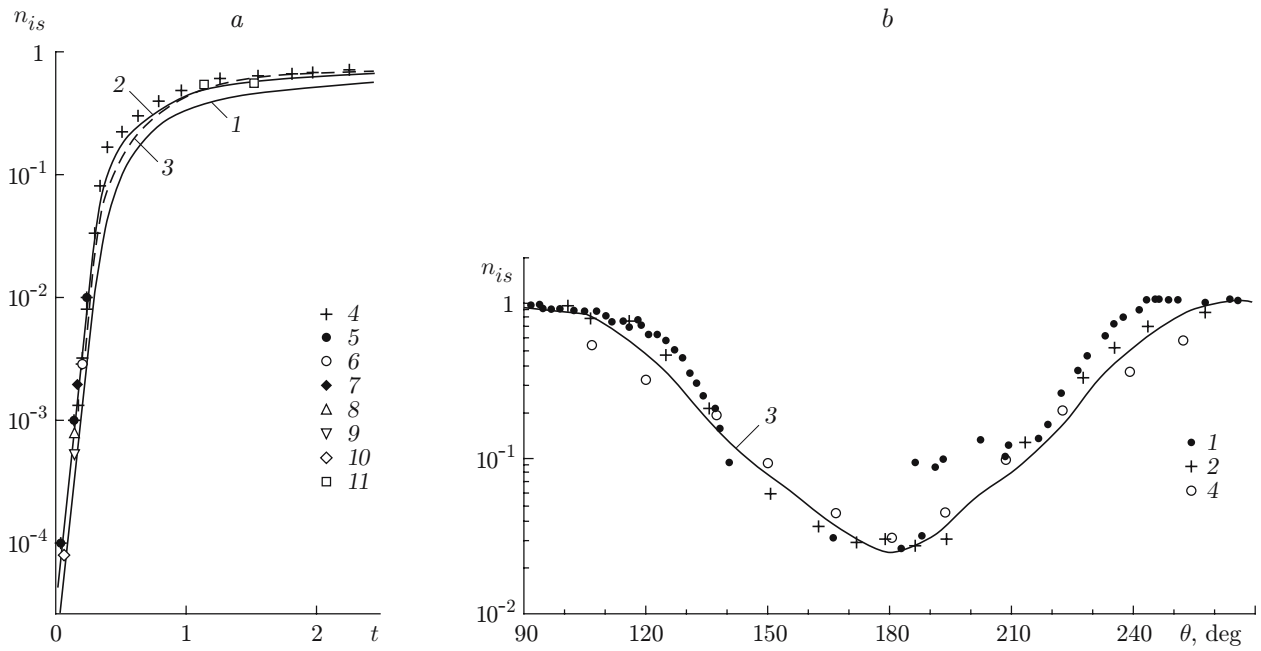


Fig. 3. Ion density distribution in the wake behind a flat solid: (a) axial distribution of $n_{is}(t)$: curves 1 and 2 are the solutions for the discrete model [11] for $\xi_{ei} = 1$ (1) and $\xi_{ei} = 4$ (2); curve 3 is the solution of Eq. (7) with the dependence $n_{is}(\Phi)$ from [6] for $S_{ei} \approx 4.1$, $R_{ds} \approx 126$, and $-\Phi_w \approx 10$; points 4 are the results measured in the present work for $S_{ei} \approx 4.1$, $R_{ds} \approx 127$, $-\Phi_w \approx 10.3$, and $\xi_{ei} = 4$; points 5 and 6 are the results calculated in [4] for $S_{ei} \approx 8$, $R_{ds} \approx 40$, and $-\Phi_w \approx 0$ (5) and 20 (6); points 7–9 are the results measured in [12] in the ionosphere on the Explorer-C (AE-C) artificial satellite for $5.9 \leqslant S_{ei} \leqslant 8.04$, $-\Phi_w \approx 10$, and $R_{ds} \approx 116.3$ (7), 135.7 (8), and 162.5 (9); points 10 are the results measured in [13] in the ionosphere on the S3-2 artificial satellite for $S_{ei} \approx 8$, $R_{ds} \geqslant 45$, and $-\Phi_w \approx 10$; points 11 are the results measured in [14] in the wake behind the Space Shuttle for $S_{ei} \approx 3.35$ and $R_{ds} \geqslant 2 \cdot 10^3$; (b) angular distribution of ion density $n_{is}(\theta)$ at $t = 0.192$: points 1 are the results measured in [12] on the Explorer-C (AE-C) artificial satellite for $S_{ei} \approx 7.83$, $R_{ds} \approx 73.4$, $-\Phi_w \approx 8.8$, and $\xi_{ei} = 1.14$; points 2 are the results measured in the present work (wake behind a cylinder for $S_{ei} \approx 5.1$, $R_{ds} \approx 78$, $-\Phi_w \approx 6.7$, and $\xi_{ei} = 4$); curve 3 is the solution of Eq. (7) with the dependence $n_{is}(\Phi)$ from [6] for $S_{ei} \approx 5.1$, $R_{ds} \approx 80$, and $-\Phi_w \approx 6.7$; points 4 are the results of the discrete flow model [11].

layer of potassium metasilicate] of thickness $\delta \approx 0.12$ cm, which was applied onto the layer of AK-512 white enamel of thickness $\delta \approx 0.08$ cm. Interaction of such models with the plasma flow is more consistent with the real situation in the ionosphere (e.g., a solar array panel or an antenna covered completely or partially by a dielectric) than the flow around a uniformly charged conducting solid. The arrangement of the experiment is shown in Fig. 4.

Figure 5 shows the cyclogram of the charging process (charge collection and neutralization) on the leeward surface of an isolated solid (TR-SO-11). The model was irradiated by a beam of high-energy electrons through a collimator, which made it possible to identify the narrow directed part of the beam and to irradiate the model-surface areas to be examined only. The cyclograms were recorded by an onboard system of contactless measurement of the probe–charge electric field strength. On segments $B$ and $C$ of the cyclogram (Fig. 5), the potential on the leeward side of a solid in a supersonic flow varies from $-\Phi_w \gg 10$ to $-\Phi_w < 10$. The regime of collection and distribution of charged particles of the "cold" plasma in the near wake behind the solid become different. The solution of Eq. (7) of the present work with the dependence $n_{is}(\Phi)$ from [6] for $-\Phi_w = 3$ and 30, $S_{ei} = 4.5$, and $R_{ds} = 67$ shows that the increase in the negative potential on the leeward surface of the solid "sweeps" the electrons of the "cold" plasma away from the near wake region and drastically increases (by 2 ot 3 orders of magnitude) the concentration of positive ions. The flow of positive ions of the "cold" plasma on the leeward surface generates by two groups of ions: $j_{iw} = j_{i\infty}^{(\mathrm{I})} + j_{i\Phi}^{(\mathrm{II})}$. The distribution of ions of group I is determined by the regime of a supersonic flow with $-\Phi_w < 10$; ions of group II penetrate into the near wake owing to their acceleration by the electric field of the charge $-\Phi_w \gg 10$ transported by high-energy electrons. As was estimated in [4], the flow around a solid with $-\Phi_w < 10$ is described by the parameter $\xi_{sh} = d_{sh}/R = 0.8\Phi_w^{3/4}/(S_{ei}^{1/2} R_{ds}) \ll 1$ ($d_{sh}$ is the thickness of the layer of the spatial charge on the frontal part of the plate or disk), while the corresponding value for the flow with

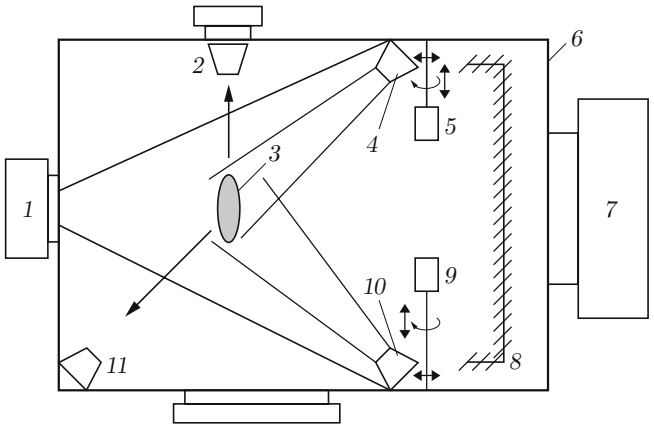


Fig. 4

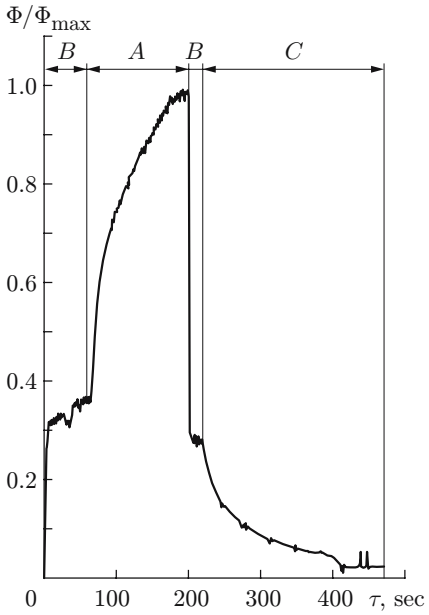


Fig. 5

Fig. 4. Arrangement of the experiment on a plasma-electrodynamic set: generator of supersonic plasma flows (1), antennas of microwave probing systems (2 and 11), solid (3), source of high-energy electrons (electron gun, voltage 0.1–35.0 keV) (4), systems of contact diagnostics of the plasma (5 and 9), vacuum chamber with a working volume of 3.5 $m^3$ (6), evacuation system (velocity of evacuation ≈100 $m^3$/sec) (7), cryogenic panels ($LN_2$) (8), and source of ultraviolet radiation of the solar spectrum in the range of 1150–7000 Å (10).

Fig. 5. Cyclogram of charging of a solid: segment A shows the radiation of the leeward surface by electrons with the energy $W_{eh}$ = 5–15 keV ($j_{eh} \approx 10$ nA/$cm^2$) without the "cold" plasma flow; segment B refers to the simultaneous action of high-energy electrons and a supersonic "cold" plasma jet; segment C illustrates neutralization of the residual charge by a supersonic "cold" plasma jet for $j_{eh} = 0$.

$-\Phi_w \gg 10$ is $\xi_{sh} \geqslant 1$. For an isolated two-sided (metal–dielectric) model (plate or disk), the "thin layer" regime is observed if there are no high-energy electrons ($-\Phi_w < 10$). If the leeward surface is irradiated by high-energy electrons, the "thin layer" regime is observed on the frontal side, and the "thick layer" regime is observed in the wake behind the solid on the leeward side ($-\Phi_w \gg 10$). For $\xi_{sh} \geqslant 1$ ("thick layer" regime), the current density of ions of the "cold" plasma on the leeward surface of the solid is determined from the condition $j_{i\infty}^{(\mathrm{I})}/j_{i\Phi}^{(\mathrm{II})} \ll 1$. The current density on the leeward surface is mainly determined by ions of group II: $j_{iw} \approx j_{i\Phi}^{(\mathrm{II})}$. In this case, the ion current density can be determined within the framework of the theory of current collection by an electric probe in a rarefied plasma. If the radius of the screening layer is large ($r_{sh}/R > \Phi_w^{1/2}/S_{ei}$ and $\Phi_w/S_{ei}^2 \gg 1$), the ion current density on the leeward side equals the current density on the probe in a motionless plasma.

In accordance with the theory of collection of the ion current by electric probes, the expression for the ion current density on the leeward side of the solid can be expressed as

$$j_{iw} = eN_{iw}(kT_{es}/(2\pi M_i))^{1/2} i_i^+(\Phi_w, R_{ds}, T_{es}/T_{is}), \tag{9}$$

where $i_i^+$ is the dimensionless strength of the ion current [7].

The uncertainty in calculating $N_{iw}$ by Eq. (9) can be avoided by using the dependences of $i_i^+$ on $(r_p/\lambda_{ds})^2 i_i^+$. For a cylindrical probe,

$$\Big(\frac{r_p}{\lambda_{ds}}\Big)^2 i_i^+ = 1.073 \cdot 10^5 \sqrt{\frac{M_i}{m_e}}\,\frac{r_p}{l_p}\Big(\frac{e}{kT_{es}}\Big)^{3/2} I_p^+(\Phi_w);$$

for a spherical probe,

$$\Big(\frac{r_p}{\lambda_{ds}}\Big)^2 i_i^+ = 5.365 \cdot 10^4 \sqrt{\frac{M_i}{m_e}}\,\Big(\frac{e}{kT_{es}}\Big)^{3/2} I_p^+(\Phi_w)$$

($I_p^+$ is the strength of the current registered by the probe; $r_p$ and $l_p$ are the probe radius and length, respectively).

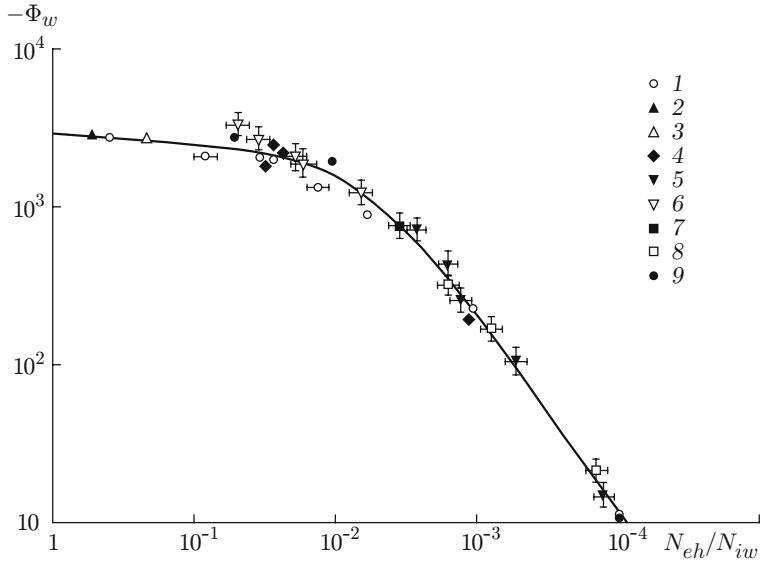


Fig. 6. Equilibrium potential on the leeward surface of a solid versus the ratio of concentrations $N_{eh}/N_{iw}$: points 1–3 are the results of ionospheric measurements [1] on F6, F7, and F13 satellites of the Defence Meteorological Satellite Program (points 1 and 2 refer to F6 and F7, respectively, for $W_{eh} \approx 4.2$, 10.1, and 14.4 keV and points 3 refer to F13 for $W_{eh} \approx 2.99$, 9.64, and 31.3 keV); points 4–8 are the experimental results of the present work for $W_{eh} \approx 5$, 10, and 15 keV for aluminum (4), VPS-7V (5), TR-SO-11 (6), stainless steel (7), and quartz (8); points 9 are the results calculated in [4] for $W_{eh} = 5$ keV.

High-voltage charging of the leeward surfaces by high-energy electrons was experimentally studied in supersonic flows of the rarefied $O^+ + O_2^+$ plasma with a concentration of charged particles $N_{i\infty} = 1.6 \cdot 10^5$–$5.7 \cdot 10^7$ cm$^{-3}$ for $T_{es} = 1.0$–$1.7$ eV and velocity $U_\infty \approx 8.4$ and 11.9 km/sec. The reference models were an isolated aluminum plate with one side covered by a dielectric and a disk made of molten quartz with one side covered by an aluminum film. The choice of aluminum as a reference material was dictated by the following circumstances:

— The values of the equilibrium potentials $\varphi_w^{\mathrm{Al}}$ measured in the present work for $W_{eh} = 5$ and 8 keV coincide with the data [3] within 1.5% and are described by a linear dependence in the range of energy $W_{eh} = 1$–$20$ keV;

— In the range of energy $W_{eh} = 1$–$20$ keV, consistent data are available for aluminum and aluminum oxide ($Al_2O_3$) on the values and dependence of the coefficients of the secondary electron emission $\sigma_{eh} = \sigma_{eh}(W_{eh})$ and secondary ion-electron emission $\gamma_i$ for the $O^+ + O_2^+$ plasma [15];

— The values of the equilibrium potential $\varphi_w$ on segments $A$ and $B$ of the charging cyclogram (see Fig. 5) for identical conditions of sample irradiation by high-energy electrons and a supersonic flow of the "cold" plasma are determined by the emission processes (values of the coefficients $\sigma_{eh}$ and $\gamma_i$ and current densities of ions $j_{iw}$ and high-energy electrons $j_{eh}$).

A comparison of the cyclograms of charging and discharging for aluminum and VPS-7V carbon plastic reveals identical values (within 3%) of $\varphi_w$ on segments $A$ and $B$ (see Fig. 5) in the range of energy $W_{eh} = 5$–$20$ keV under identical test conditions. This fact shows that the emission processes are identical, the coefficients $\sigma_{eh}$ and $\gamma_i$ for one kind of ions of the "cold" plasma are equal to each other, and the ion current densities on the leeward surface of the solid $j_{iw}$ are also identical.

For all dielectrics and for each fixed value of $W_{eh}^{(1)}$, the coefficient of the secondary electron emission $\sigma_{eh}^{di}$ can be determined on the basis of segment $A$ of the cyclogram (see Fig. 5) with the use of the linear dependence $\varphi_{\mathrm{Al}}(W_{eh})$, the condition $\varphi_{di}^{(A)}(W_{eh}^{(1)}) = \varphi_{\mathrm{Al}}(W_{eh}^{(2)})$, and the dependence $\sigma_{eh}^{\mathrm{Al}}(W_{eh})$ from [15]: $\sigma_{eh}^{di}(W_{eh}^{(1)}) = \sigma_{eh}^{\mathrm{Al}}(W_{eh}^{(2)})$ and $\sigma_{eh}^{di} = \sigma_{eh}(W_{eh})$. If $\varphi_{\mathrm{Al}}^{(B)}(W_{eh}^{(1)}) \neq \varphi_{di}^{(B)}(W_{eh}^{(1)})$ on segment $B$ of the cyclogram for fixed values of parameters of the beam of high-energy electrons in one flow of the "cold" rarefied plasma, one can choose an appropriate regime of dielectric irradiation by high-energy electrons in the same "cold" plasma flow and obtain a flow regime with $\varphi_{\mathrm{Al}}^{(B)}(W_{eh}^{(1)}) \approx \varphi_{di}^{(B)}(W_{eh}^{(2)})$ and, as a consequence, $j_{iw}^{\mathrm{Al}} \approx j_{iw}^{di}$. The value of $j_{iw}^{\mathrm{Al}}$ for aluminum can be estimated by Eq. (3). Using the condition $j_{iw}^{\mathrm{Al}} \approx j_{iw}^{di}$, we can apply Eq. (3) to estimate the coefficient of the secondary ion-

electron emission $\gamma_i^{di}$ for an ion flow with the energy approximately equal to $e\varphi_{di}^{(B)}$. Such a procedure was used for the TR-SO-11 coating.

Aluminum and VPS-7V carbon plastic, aluminum and TR-SO-11 coating, stainless steel and VPS-7V, and aluminum and quartz were alternatively used as the frontal and leeward surfaces in experiments. A negative equilibrium potential $-\varphi_w > 200$ V was established on the leeward surface of the model, and $\varphi_f \ll \varphi_w$ on the frontal surface. The "thick layer" regime was obtained in the near wake behind the solid for $3.1 \leqslant S_{ei} \leqslant 4.5$, $14 \leqslant R/\lambda_{ds} \leqslant 35$, and 1.0 eV $\leqslant T_{es} \leqslant 1.7$ eV.

Figure 6 shows the equilibrium potential $-\Phi_w$ on the leeward side of the solid as a function of the ratio of concentrations of high-energy electrons and positive ions on the leeward surface $N_{eh}/N_{iw}$. The limiting value $N_{eh}/N_{iw} \approx 10^{-4}$ corresponds to numerical estimates of the level of microsatellite charging in the wake behind a flat solid in the polar plasma [4].

**Conclusions.** A procedure for modeling high-voltage charging of surfaces of solids by high-energy electrons in a polar plasma of the ionosphere is developed. The dependences $-\Phi_w = \Phi_w(N_{eh}/N_{iw})$ obtained make it possible to predict the levels of charging of the leeward surfaces of the solid in a supersonic rarefied plasma flow.

## REFERENCES


1. M. A. Gussenhoven, D. A. Hardy, F. Rich, et al., "High-level spacecraft charging in the low-altitude polar and auroral environment," *J. Geophys. Res.*, **90**, No. A11, 11009–11023 (1985).
2. A. V. Gurevich, L. P. Pitaevskii, and V. V. Smirnova, "Ionospheric aerodynamics," *Usp. Fiz. Nauk*, **99**, No. 1, 3–49 (1969).
3. V. M. Antonov and A. G. Ponomarenko, *Laboratory Research of Electrization Effects for Space Vehicles* [in Russian], Nauka, Novosibirsk (1992).
4. J. Wang, P. Lenng, A. Garrett, and G. Murphy, "Multibody-plasma interactions: charging in the wake," *J. Spacecraft Rockets*, **31**, No. 5, 889–894 (1994).
5. V. A. Shuvalov and É. A. Zel'dina, "Structure of the electrostatic field in the wake behind a sphere in an equilibrium rarefied plasma flow," *Geomagnetism Aéronomiya*, **16**, No. 4, 603–607 (1976).
6. V. C. Liu, "Ionospheric gas dynamics of satellite and diagnostic probe," *Space Sci. Rev.*, **9**, 423–490 (1969).
7. V. A. Shuvalov, G. S. Kochubei, A. I. Priimak, et al., "Contact diagnosing of high-velocity rarefied plasma flows," *Teplofiz. Vysok. Temp.*, **43**, No. 3, 343–351 (2005).
8. I. M. Bronshtein and B. S. Fraiman, *Secondary Electron Emission* [in Russian], Nauka, Moscow (1969).
9. G. Fournier and D. Pigache, "Wakes in collisionless plasma," *Phys. Fluids*, **18**, No. 11, 1443–1453 (1975).
10. H. Kozima, K. Yamada, and K. Nakasima, "The self-similarity and the non-neutrality of near-wakes in two-dimensional geometry," *Phys. Fluids B*, **1**, No. 4, 719–724 (1989).
11. A. V. Gurevich and V. V. Smirnova, "Supersonic rarefied plasma flow around flat solids," *Geomagnetism Aéronomiya*, **10**, No. 3, 402–407 (1970).
12. U. Samir, R. Gordon, L. Brace, and R. Theis, "The near-wake structure of the Atmosphere Explorer C (AE-C) satellite. A parameter investigation," *J. Geophys. Res.*, **84**, No. A2, 513–525 (1979).
13. U. Samir, P. Weldman, F. Rich, et al., "About the parametric interplay between ionic Mach number, body-size and satellite potential in determining the ion depletion in the wake of the S3-2 satellite," *J. Geophys. Res.*, **86**, No. A13, 11161–11166 (1981).
14. G. B. Murphy, D. L. Reasoner, A. Tribble, et al., "The plasma wake of the Shuttle orbiter," *J. Geophys. Res.*, **94**, No. A6, 6866–6872 (1989).
15. L. V. Nosachev and V. V. Skvortsov, "Investigation of the ion current distribution in the wake behind cylindrical and spherical solids in argon and nitrogen plasma flows," *Uch. Zap. TsAGI*, **1**, No. 5, 39–44 (1970).